RSC Advances

PAPER

View Article Online
View Journal | View Issue

Cite this: *RSC Adv.*, 2026, **16**, 18657

Effective extraction and determination of 9 β-lactams in water and milk samples by a novel magnetic covalent organic framework combined with UPLC-MS/MS

Lu Li,[ab] Na Li,[a] Wendan Niu,[ab] Aijing Guo,[ab] Ling Ma,*[ab] Wei Zhao,*[a] Yawei Zhang*[a] and Ke Wang *[ab]

Received 2nd December 2025
Accepted 23rd March 2026

DOI: 10.1039/d5ra09307d

rsc.li/rsc-advances

β-Lactams (β-LAs) are a class of widely used antibiotics. However, their residues in food may pose a threat to human health. Therefore, it is of great necessity to develop a method that can sensitively and effectively detect β-LAs at trace levels in complex matrices. In this study, a novel functionalized magnetic covalent organic framework was synthesized based on biphenyl-3,3′,5,5′-tetracarbaldehyde and *p*-phenylenediamine. This material was used as an adsorbent for the effective extraction of 9 β-LAs in water and milk samples, which were analyzed by ultra-performance liquid chromatography-tandem mass spectrometry (UPLC-MS/MS). The experimental parameters were optimized, then the sensitive and accurate detection method was developed with excellent linearity ($R^2 \geq 0.9990$), low limits of detection (0.001–0.347 μg L^{-1}) and limits of quantitation (0.002–1.051 μg L^{-1}) for β-LAs. Meanwhile, good recoveries (71.7–118.8%) of 9 β-LAs in water and milk samples were obtained with the relative standard deviations (RSD) <10% ($n = 5$). In conclusion, Fe_3O_4@SiO_2@Ap-COF can be regarded as an effective magnetic adsorbent, and the established method holds significant promise for rapid detection of 9 β-LAs in water and milk samples.

1 Introduction

β-Lactam antibiotics (β-LAs) constitute a class of important antibacterial drugs containing β-lactam rings, mainly including penicillins and cephalosporins.[1] In recent years, β-LAs have found widespread use for the prevention or treatment of bacterial infections, accounting for roughly two-thirds of commonly administered antibiotics owing to their broad-spectrum activity, low toxicity, and cost-effectiveness.[2]

However, when animals ingest β-lactam antibiotics, these drugs and their metabolites accumulate in animal organs and tissues, this retention could pose risks to public health.[3,4] On the one hand, β-LAs can lead to water pollution through the excretion of animal feces and the discharge of wastewater from livestock farms and pharmaceutical factories.[5] On the other hand, unmetabolized antibiotics in the animal's body can migrate into animal derived foods, such as milk, eggs, fish and meat, posing health risks to consumers. Milk is one of the most consumed foods owing to its rich content of essential nutrients. However, cephalosporins are widely used as feed additives in veterinary medicine, which may compromise the quality of milk.[6] Therefore, regulatory authorities and institutions including the European Commission, China, and the United States have established maximum residue limits (MRLs) for β-LAs in foods of animal origin to safeguard consumer safety. In view of this, it is crucial to develop sensitive, reliable and simple analytical methods for the monitor of β-LAs in water and milk samples to ensure public health security.

Current methods for β-LAs analysis are based on capillary electrophoresis (CE),[7] enzyme-linked immunosorbent assay,[8] liquid chromatography (LC),[9] chemiluminescence methods,[10] and liquid chromatography-tandem mass spectrometry (LC-MS/MS).[11] Among these methods, LC-MS/MS has been well adopted owing to its high sensitivity, high specificity, high-throughout qualitative and quantitative analysis. Due to the complex matrix in the actual sample, which contains many potential interference components, simple and effective sample pretreatment is critical before analysis and detection. Commonly used sample pretreatment methods include liquid–liquid extraction (LLE),[12] molecular imprinting technology,[13] pressurized liquid extraction,[14] matrix solid-phase dispersion (MSPD),[1] solid phase extraction (SPE),[15,16] and QuECHERS.[17,18]

Different from the traditional sample pretreatment methods, magnetic solid-phase extraction (MSPE) is an advanced technique based on dispersed solid-phase extraction,

[a]*Shijiazhuang Center for Disease Control and Prevention, Shijiazhuang 050011, China. E-mail: mamalin001@163.com; 13933887009@139.com; 2211291167@qq.com*

[b]*Shijiazhuang Technology Innovation Center for Chemical Poison Detection and Risk Early Warning, Shijiazhuang 050011, China. E-mail: wkecdc@163.com*

which uses a magnetic adsorbent for the separation and enrichment of analytes *via* an applied magnetic field. The magnetic adsorbent is a magnetic nanocomposite with a core–shell structure, which is formed by combining a magnetic nanoparticle (MNPs) core with a non-magnetic adsorptive material. Since MSPE has the characteristics of an easy, green, environmental-friendly and effective extraction approach, it has received great attention for complex sample preparation in recent years.[19] Among them, Fe_3O_4 is the most common MNPs because of advantages of high magnetic moments, good biocompatibility, simple preparation methods, and low production costs.[20] Various materials including carbon nanotubes (CNTs), graphene,[21,22] molecularly imprinted polymers (MIPs),[23] and metal–organic frameworks (MOFs),[24,25] have been explored as MSPE adsorbent materials. Covalent organic frameworks (COFs) are a new type of porous polymers, which have attracted extensive attention due to their excellent properties of large specific surface area, unique topological structure, high thermochemical stability and functional modification.[26–28] COFs exhibit a high affinity for target compounds and can extract a wide range of pollutants, including pesticides, polycyclic aromatic hydrocarbons (PAHs), antibiotics, heavy metal ions, illegal additives, hormones, and biotoxins.[29–33] Compared with MIPs, COFs possess a higher specific surface area, porosity, mass transfer limitations, and adsorption capacity.[34,35] Besides, compared with MOFs, COFs have been proved to be more stable in water and acidic media.[36,37] However, since the sizes of COFs are typically in the micro- and nano-scale, it is difficult to precipitate COFs with low density from complex matrix.[38]

Fascinatingly, the combination of COFs and Fe_3O_4 effectively makes up for this limitation, not only possess high adsorption capacity, but also facilitate separation.[33,39]

In recent years, a large number of literature have reported the application of magnetic materials in the separation of macromolecular substances,[40] organic compounds[41] and metal ion enrichment.[42] Some studies have shown that magnetic materials have great potential in extracting antibiotics from water samples, such as the detection of tetracycline drugs,[43] the extraction of sulfonamides,[44] but there are few applications in the detection of β-LAs. Most reported MSPE methods employ molecularly imprinted polymers (MIPs) as the magnetic adsorbent,[13,45,46] In contrast, the use of magnetic covalent organic frameworks (COFs) is rare. Furthermore, these methods are often limited to a single sample matrix and cover only a small number of target analytes.

In the present study, a novel adsorption material was synthesized by using silanized Fe_3O_4 as the core of the magnetic material and COFs formed by the combination of 3,3′,5,5′-tetraldehyde-biphenyl and *p*-phenylenediamine as the shell of the magnetic material. The obtained Fe_3O_4@SiO_2@Ap-COF was used as an MSPE adsorbent and combined with UPLC-MS/MS for the enrichment of 9 kinds of β-LAs, demonstrating excellent adsorption performance. Subsequently, the main parameters influencing the MSPE procedure were optimized and the developed method was validated.

2 Experimental

2.1 Reagents and materials

Ferric chloride hexahydrate ($FeCl_3 \cdot 6H_2O$), ethylene glycol (EG), sodium acetate anhydrous (NaAc), 1,4-dioxane, aodium chloride (NaCl) and anhydrous ethanol were obtained from Tianjin Yong da Chemical Reagent Ltd (Tianjin, China). Biphenyl-3,3′,5,5′-tetracarbaldehyde and *p*-phenylenediamine were purchased from Shanghai Macklin Biochemical Ltd (Shanghai, China). Tetraethoxysilane (TEOS) was sourced from Aladdin Chemistry Ltd (Shanghai, China). Polyethylene glycol (PEG-4000) was supplied by Xiya Chemical Technology Ltd (Shandong, China). 37% (w/w) hydrochloric acid were acquired from Tianjin Kernel Chemical Reagent Ltd (Tianjin, China). Acetonitrile (ACN) was purchased from Sigma-Aldrich (St. Louis, MO, USA), methanol (MA), hexane and ethyl acetate were procured from Thermo Fisher Ltd (Waltham, USA). Formic acid (FA) was purchased from Dikma (Lake Forest, USA). Superior pure dichloro-methane was purchased from Tianjin Kemiou Chemical Reagent (China). Formic acid, acetonitrile and methanol were HPLC grade, whereas the remaining reagents were analytical grade. The ultrapure water was manufactured using a Milli-Q purification system (Millipore, Bedford, USA).

Cefpiramide acid (CRA), cefoperazone (CFP), ceftiofur (EFT), cefpodoxime proxetil (CPD), cefetamet pivoxil hydrochloride (CETP), dicloxacillin sodium (DIC), flucloxacillin (FLU), cloxacillin (CLO), and oxacillin sodium (OXA) were obtained from Alta Scientific Co., Ltd (Tianjin, China). The properties of β-LAs of all standards were shown in Table S1.

2.2 Instrumental and analytical conditions

The UPLC-MS/MS instrument (Exion TRILPLE QUAD 5500, AB SCIEX, USA) was used to determine analytes. Chromatographic separation was performed on an Agilent ZORBAX SB-Aq column (2.1 × 150 mm, 3.5 μm). The injection volume was 5 μL and a constant flow rate of 0.5 mL min^{-1} was maintained. Mobile phase A was 0.1% formic acid aqueous solution, while mobile phase B was ACN. The gradient elution program was set as follows: (1) 0–1.0 min, 30% B (v/v); (2) 1.1–4.0 min, 40% B (v/v); (3) 4.1–6.0 min 70% B (v/v); (4) 6.1–7.0 min 85% B (v/v); (5) 7.1–10.0 min 30%, B (v/v). The column temperature was set at 40 °C. Mass spectrometric analysis was conducted in multiple reaction monitoring (MRM) mode using an electrospray ionization source (ESI) in the positive ion mode. The mass spectrometry parameters have been configured, including spray voltage (5500 V), vaporizer temperature (550 °C), nebulizing gas pressure (55 psi), auxiliary gas pressure (55 psi), and curtain gas pressure (40 psi). In addition, the other parameters including retention times, precursor ion and product ion mass, declustering potential (DP) and collision energy (CE) were listed in Table S2. Besides, the chromatograms of 9 β-LAs were listed in Fig. S1.

Fourier infrared transform (FT-IR) spectras were obtained *via* a Nicole iS5 spectrometer (Thermo Nicolet Co. Ltd, USA). The Brunauer–Emmett–Teller (BET) surface areas were measured by Quadrasorb EVO (Quantachrome Instruments, USA). The X-ray diffraction (XRD) graphs were acquired using a German Bruker

D8 (Bruker, Germany). The magnetizations of the materials were determined by a SQUID XL-7 vibrating sample magnetometer (Quantum Design, USA). Morphology of the materials were observed using a Regulus 810 scanning electron microscopy (SEM, Hitachi, Japan) and a FEI Tecnai G2 F20 transmission electron microscope (TEM, FEI, USA).

2.3 Preparation of magnetic adsorbents

2.3.1 Synthesis of the Fe_3O_4 nanoparticles. The magnetic Fe_3O_4 nanoparticles were synthesized by the previously reported solvent thermal method.[47,48] Specifically, 1.62 g of $FeCl_3 \cdot 6H_2O$ was dissolved in 60 mL of ethylene glycol (EG) under vigorous stirring at room temperature. Then, 7.2 g of $CH_3COONa \cdot 3H_2O$ and 2.0 g of PEG-4000 were added into the solution. After stirring for 30 min, the above-yellow solutions were transferred into the Teflon-lined autoclave, heated at 200 °C for 8 h. After cooling to room temperature, the black product was separated using a magnet, washed several times with absolute ethanol and pure water, and then dried at 60 °C for 4 h in a vacuum for subsequent use.

2.3.2 Synthesis of Fe_3O_4@SiO_2. The obtained Fe_3O_4 magnetic nanoparticles were further coated with a SiO_2 layer through the sol–gel method.[49,50] 200 mg as-prepared Fe_3O_4 nanoparticles were dispersed in a mixed solution consisted of 160 mL anhydrous ethanol and 40 mL ultrapure water. Next, the mixture was sonicated for 30 min to ensure uniform dispersion. Then, 3 mL of 25% (w/w) ammonia was added into the mixture, followed by 5 min of sonication. Furtherly, 2 mL of tetraethoxysilane (TEOS) was added slowly dropwise under stirring, the mixture was stirred for 24 h at 30 °C, then the precipitation was washed with anhydrous ethanol and ultrapure water for several times, dried under vacuum at 60 °C for 4 h. As a result, the Fe_3O_4@SiO_2 was obtained.

2.3.3 Synthesis of Fe_3O_4@SiO_2@Ap-COF. 150 mg of Fe_3O_4@SiO_2 magnetic particles were accurately weighed into a 100 mL round-bottom flask containing 20 mL 1,4-dioxane solvent. The mixture was dispersed evenly by ultrasound, after that the round-bottom flask was placed into an oil bath agitator. Next, 80 mg biphenyl-3,3′,5,5′-tetracarbaldehyde (0.30 mmol) was dissolved in 10 mL of DMSO by ultrasound for 1–2 min, and uniformly added to the flask. After the drip was completed, another 10 mL 1,4-dioxane solvent was added to the test tube, and then uniformly added to the flask. Similarly, *p*-phenylenediamine (64.88 mg, 0.60 mmol) was dissolved in 5 mL 1,4-dioxane solvent first, followed by ultrasound, and uniformly added to the flask, and then 5 mL 1,4-dioxane was added to the test tube. Finally, 0.5 mL 12 M acetic acid solution was first added to the mixture, and then 4.5 mL 12 M acetic acid solution was added to the mixture after 2 h, and the reaction was heated at 70 °C for 24 h. A two-step addition of acetic acid was employed to reduce the reaction rate, which prevented an excessively fast reaction from promoting the organic compounds to self-polymerize into discrete COFs, rather than coating the Fe_3O_4@SiO_2 magnetic cores. This approach facilitated the formation of a uniform core–shell structure. At the end of the reaction, the reaction products were cooled to room temperature, separated by magnets, washed with 1,4-dioxane solvent and anhydrous ethanol for 2–3 times, and dried in vacuum at 60 °C for 3 h to obtain Fe_3O_4@SiO_2@Ap-COF.

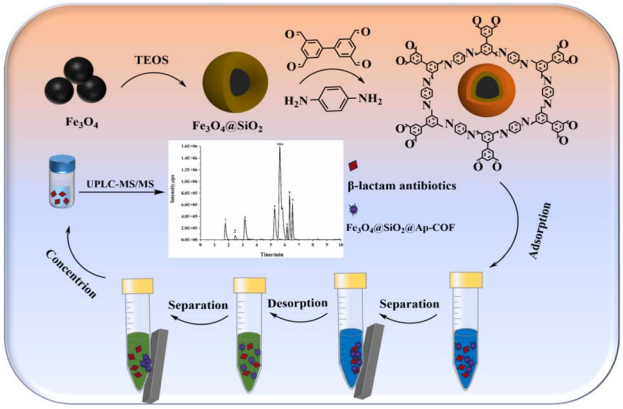

Scheme 1 Synthetic process for Fe_3O_4@SiO_2@Ap-COF and MSPE procedure.

2.4 Collection and sample preparation

20 water samples were collected from different rivers during autumn in Shijiazhuang City, China, which were filtered by 0.45 μm filter membrane and stored 4 °C. Before MSPE, the sample solution pH was adjusted to 3.0 with dilute hydrochloric acid.

15 milk samples (10 whole milk samples and 5 skimmed milk samples) were purchased from local supermarkets during autumn in Chang'an District, Shijiazhuang City, China. Before MSPE, 1.0 g of the homogenized sample was transferred to a 50 mL centrifuge tube, then 12 mL acetonitrile–water (3 : 1, v/v) was added and vortexed for 3 min to extract β-LAs. After centrifuged for 5 min at 4 °C under 10 000 rpm, 6 mL aliquot supernatant was added into a 15 mL centrifuge tube, and dried under nitrogen at 40 °C. Subsequently, the dried residue was dissolved in 10 mL of ultra-pure water, and the pH was adjusted to 3.0 with dilute hydrochloric acid before MSPE.

2.5 Procedure of MSPE

The extraction procedure is depicted in Scheme 1. Specifically, 10 mL of sample solution and 8 mg of Fe_3O_4@SiO_2@Ap-COF were added to a 50 mL centrifuge tube. The mixture was subjected to 15 min of intense vortexing for adsorption, followed by separating the material from the solution using a magnet. 8 mL 0.3% (v/v) acidified methanol was added to desorb the β-LAs from Fe_3O_4@SiO_2@Ap-COF by vortex for 7 min, and the eluent obtained was filtered through a 0.20 μm filter for HPLC-MS/MS analysis. In addition, the magnetic material Fe_3O_4@SiO_2@Ap-COF was vibrately washed several times with 0.3% acidified methanol and recycled after vacuum drying at 60 °C.

3 Results and discussions

3.1 Characterization of the Fe_3O_4@SiO_2@Ap-COF

The SEM and TEM images revealed the structural characteristics of Fe_3O_4 nanoparticles and Fe_3O_4@SiO_2@Ap-COF

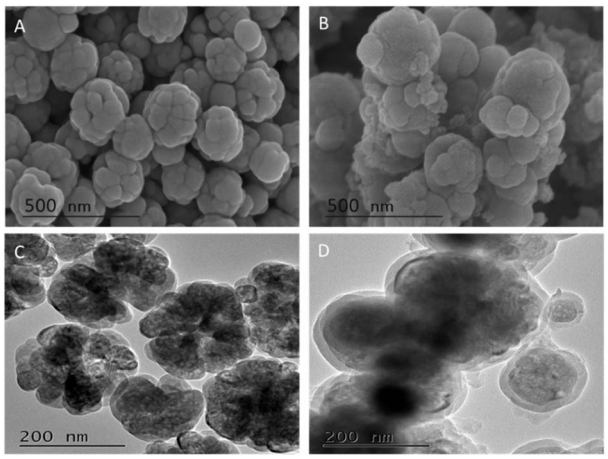

Fig. 1 The SEM of (A) Fe_3O_4, (B) Fe_3O_4@SiO_2@Ap-COF; the TEM of (C) Fe_3O_4, (D) Fe_3O_4@SiO_2@Ap-COF.

nanoparticles. As shown in Fig. 1A and B, it can be seen that Fe_3O_4 had a smooth and well-dispersed surface, while Fe_3O_4@SiO_2@Ap-COF had a rough surface. The typical core–shell structure, comprising a Fe_3O_4 nanoparticle core and a gray COF layer, can be clearly observed in the TEM images presented in Fig. 1C and D. Besides, based on SEM, the average particle diameter of Fe_3O_4 was approximately 55 nm, while that of Fe_3O_4@SiO_2@Ap-COF was about 66 nm, which showed the formation of a coating shell with thickness of approximately 11 nm, further approving the successful coating of COF.

To further prove the successful synthesis of Fe_3O_4@SiO_2@Ap-COF, the crystalline structures and characteristic spectrum of Fe_3O_4, Fe_3O_4@SiO_2 and Fe_3O_4@SiO_2@Ap-COF were determined through XRD and FT-IR.

The scanning FTIR images of the Fe_3O_4@SiO_2@Ap-COF revealed that synthesis process of Fe_3O_4@SiO_2@Ap-COF. As depicted in Fig. 2A, the typical band at 587 cm^{-1} was assigned to the Fe–O–Fe vibration. The broad bands of –OH at 3432 cm^{-1} and 1637 cm^{-1} could be classified as the stretching and bending vibrations of water molecules on the surface of Fe_3O_4. The peaks around 1105 cm^{-1} were induced by the Si–O bending vibration, indicating that the silica shells were successfully coated on the surface of Fe_3O_4. Furthermore, the emerging stretching at 1504 cm^{-1} and 1626 cm^{-1} was caused by the benzene skeleton of C=C stretching and the C=N stretching vibrations,[51] which show the successful coating of COFs on the surface of Fe_3O_4@SiO_2 by Schiff-base condensation reaction. The FT-IR results confirmed the successful fabrication of Fe_3O_4@ SiO_2@Ap-COF.

As seen in Fig. 2B, all the synthesized MNPs had the same peaks at wide angles ($2\theta = 30.01°$, 35.49°, 42.98°, 53.43°, 56.92°, and 62.53°), Corresponding to (220), (311), (400), (422), (511) and (440) in the standard magnetite XRD pattern (JCPDS 19-0629).[39] The results show that Fe_3O_4@SiO_2@Ap-COF has good crystallization and high crystallinity after coating, and the crystalline phase of Fe_3O_4 was well maintained during the synthesis of the Fe_3O_4@SiO_2 and Fe_3O_4@SiO_2@Ap-COF. The VSM was used to further validate the magnetic behaviors of Fe_3O_4 and Fe_3O_4@SiO_2@Ap-COF. The magnetization of the material was the key factor in the rapid separation of the adsorbent from the sample solution. As depicted in Fig. 2C, the saturation magnetization values of the Fe_3O_4 and Fe_3O_4@SiO_2@Ap-COF were 79.12 and 40.43 emu g^{-1}, respectively. Compared with Fe_3O_4, the Fe_3O_4@SiO_2@Ap-COF showed a significant decrease in saturation magnetization, which could be due to the shielding effect of the coated layer on the

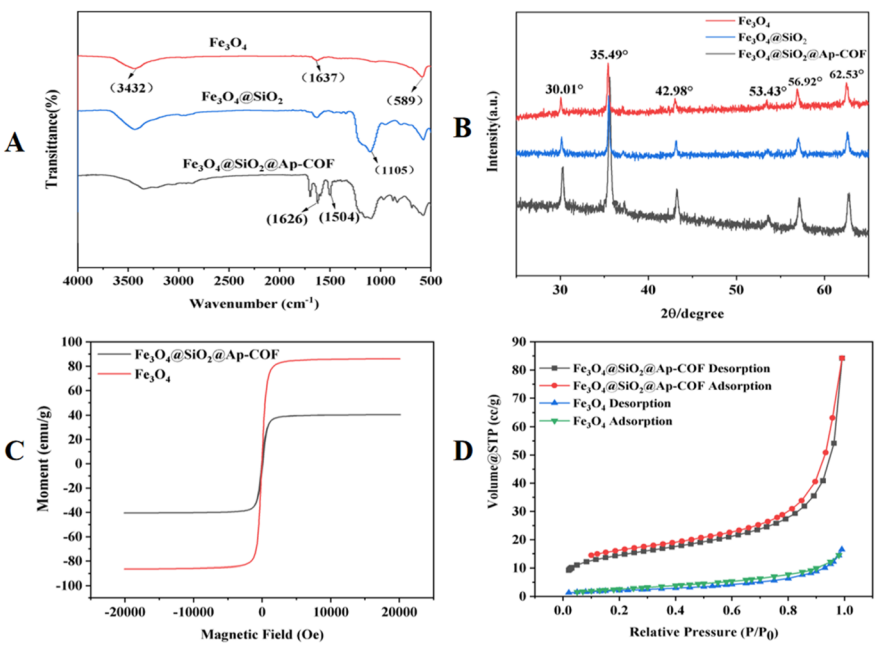

Fig. 2 (A) FT-IR spectra of Fe_3O_4, Fe_3O_4@SiO_2 and Fe_3O_4@SiO_2@Ap-COF. (B) XRD analysis of Fe_3O_4, Fe_3O_4@SiO_2, and Fe_3O_4@SiO_2@Ap-COF. (C) VSM magnetization curves of Fe_3O_4 and Fe_3O_4@SiO_2@Ap-COF. (D) N_2 adsorption–desorption isotherms of Fe_3O_4, and Fe_3O_4@SiO_2@Ap-COF.

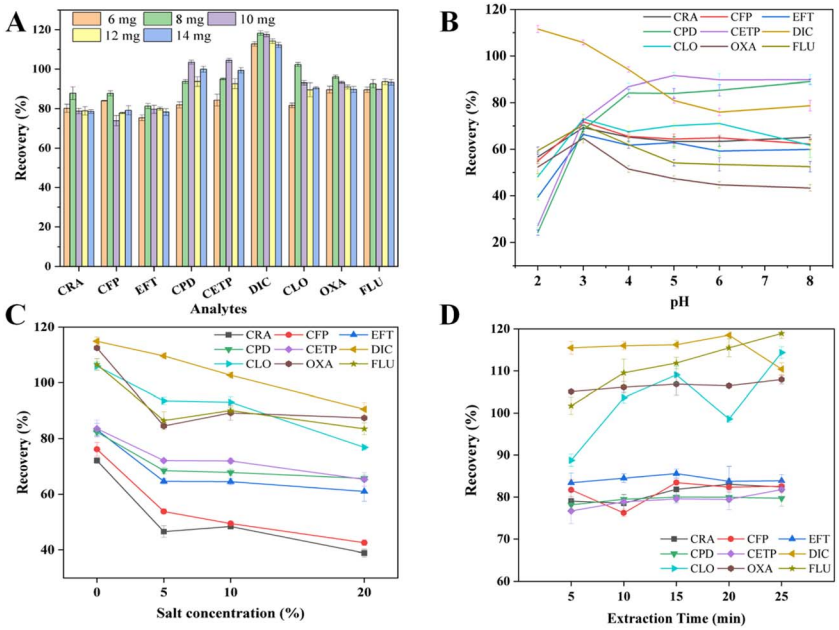

Fig. 3 Effect of (A) adsorbent dosage; (B) sample solution pH; (C) salt concentration; (D) extraction time.

magnetization of the Fe_3O_4, further confirming the successful coating of the COF material. However, under an external magnetic field, the magnetization of Fe_3O_4@SiO_2@Ap-COF can still ensure the rapid separation of it from liquid samples within 1 min.

The porosity and surface area was investigated *via* N_2 adsorption–desorption analysis at 77 K. As presented in Fig. 2D, Fe_3O_4 is a type II adsorption isotherm,[52] and Fe_3O_4@SiO_2@Ap-COF shows a type IV adsorption isotherm. After calculation, the BET surface area of Fe_3O_4@SiO_2@Ap-COF was 52.32 m^2 g^{-1}, which was higher than that of the Fe_3O_4 with a surface area of 7.89 m^2 g^{-1}. A high specific surface area facilitated contact between the material and analyte, thereby providing more available adsorption sites and consequently enhancing adsorption performance of material toward β-LAs. Compared with Fe_3O_4, Fe_3O_4@SiO_2@Ap-COF possesses a higher specific surface area, which gives it an advantage in adsorbing β-LAs. All these results demonstrated that the Fe_3O_4@SiO_2@Ap-COF was suitable for acting as an adsorbent for β-LAs with high adsorption efficiency.

3.2 Optimization of MSPE condition

To achieve high extraction efficiency, some influencing factors such as adsorbent dosage, sample solution pH, salt concentration, extraction time, type and volume of the desorption solvent, and desorption time were optimized in detail. Such optimization experiments were performed using single factor approach.

3.2.1 Effect of adsorbent dosage. The amount of Fe_3O_4@SiO_2@Ap-COF is a key factor to affect the extraction efficiency in MSPE process. Various amounts of MSPE were investigated over the range of 6 to 14 mg. As displayed in Fig. 3A, the extraction recoveries of the 9 β-LAs increased rapidly as the adsorbent dosage increased from 6 to 8 mg and then a slowdown in upward trend was observed with the recovery rates of some drugs even decreasing slightly. The possible reason is that the adsorbent supplies high specific surface area and sufficient adsorption sites,[53] which enables even a small dosage of Fe_3O_4@SiO_2@Ap-COF is capable of capturing target analytes. Therefore, 8 mg was utilized for the following experiments.

3.2.2 Effect of sample solution pH. Since the basic structure of β-LAs contains acidic or alkaline functional groups, the pH value of the solution has a significant impact on the extraction efficiencies of the analytes.[54] In this study, the pH of the solution was adjusted by adding an appropriate amount of hydrochloric acid or sodium hydroxide, and the extraction effect was investigated in the pH range of 2.0–8.0. As displayed in Fig. 3B, when the pH was 2, the recoveries of most β-LAs were all lower than 60%, while the pH was 3, Fe_3O_4@SiO_2@Ap-COF had the best overall extraction effect on 9 β-LAs, and the recoveries ranged from 64.7% to 105.8%. However, when pH was higher than 3, the recoveries of most β-LAs were decreased. Therefore, the optimal pH is 3.

3.2.3 Effect of salt concentration. The ionic strength of the solution influences analyte solubility and plays a critical role in their distribution between the organic and aqueous phases. The effect of ionic strength was evaluated through the addition of NaCl at different concentrations (0–20%, w/v) to samples. As displayed in Fig. 3C, with the increase of NaCl concentration, the recoveries of these 9 β-LAs compounds showed a significant downward trend. The possible reason is that NaCl occupies the adsorption site on the surface of Fe_3O_4@SiO_2@Ap-COF. Moreover, the increase of NaCl concentration led to higher solution viscosity and lower diffusion rates, thereby reducing the extraction efficiency of β-LAs.[55] Thus, NaCl was not used in MSPE procedure.

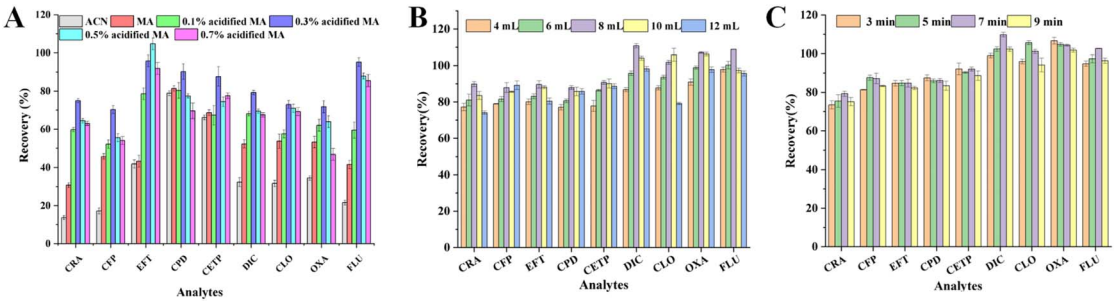

Fig. 4 Effect of different (A) elution solvents; (B) elution volume; (C) desorption time.

3.2.4 Effect of extraction time. The extraction time influences the distribution equilibrium of β-LAs between the adsorbents and the sample solution.[56] In this study, different extraction time was investigated ranging from 5 to 25 min. As displayed in Fig. 3D, the overall recovery of analytes was the best at 15 min, all of which were higher than 80%, and the adsorption equilibrium was reached after 15 min, with no significant change in adsorption efficiency. Therefore, 15 min was selected as the optimal extraction time.

3.2.5 Investigation of desorption parameters. During the MSPE procedure, the eluent, eluent volume and elution time are key factors affecting desorption of the target analytes.

The eluent is an important factor to obtain good desorption efficiency. Therefore, the elution effect of MA and ACN was first investigated. As seen in Fig. 4A, the elution effect of MA is significantly better than that of ACN. Additionally, the addition of an appropriate amount of acidic solution facilitates the separation of analytes. Therefore, the effect of methanol acidification was further investigated. When the concentration of formic acid was 0.3% (v/v), the highest overall elution efficiency for the nine analytes was achieved, with recoveries ranging from 70.3% to 95.8%. However, the elution efficiency gradually decreased as the formic acid concentration in the methanol increased. We speculate that this decline is because that the chemical structure of β-LAs may easily destroyed under acidic environment.[57] Therefore, 0.3% (v/v) acidified MA was selected for elution.

Notably, the volume of the eluent influenced the recoveries of the analytes. In this study, different eluent volumes (4 mL, 6 mL, 8 mL, 10 mL, 12 mL) were investigated. As presented in Fig. 4B, when eluent volume was 8 mL, the recoveries of 9 β-LAs were optimal, in the range of 87.9–110.8%.

Additionally, when the elution volume was fixed, the effects of different elution time on β-LAs were further explored from 3 to 9 min. Fig. 4C showed that when the vortex time was 7 min, the recoveries of 9 β-LAs reached the best level (79.2–109.8%), and the recoveries did not significantly alter with the increase of the vortex time. Therefore, the elution time of 7 min was selected in this study.

3.3 Adsorption mechanism

C=N group and benzene ring of the Fe_3O_4@SiO_2@Ap-COF could form the large π-conjugation system, which was prone to induce π–π interaction with β-LAs containing carbonyl group and benzene ring.[58]

Furthermore, Fe_3O_4@SiO_2@Ap-COF exhibited optimal adsorption performance for β-LAs at pH 3. This could be attributed to the fact that pK_a values of most β-LAs were close to 3, then β-LAs predominantly existed in original state at pH 3. Correspondingly, the abundant N atoms of the Fe_3O_4@SiO_2@Ap-COF could interact with carboxyl group, hydroxyl group or amino group of β-LAs *via* hydrogen bond, thereby achieving efficient adsorption.

Hydrophilicity and hydrophobicity are related to the log *P* value[59,60] (the higher log *P* value, the better hydrophobicity). The log *P* values of most β-LAs were above 1, indicating their good hydrophobicity. Meanwhile, the Fe_3O_4@SiO_2@Ap-COF contained abundant benzene rings, increasing the hydrophobicity.

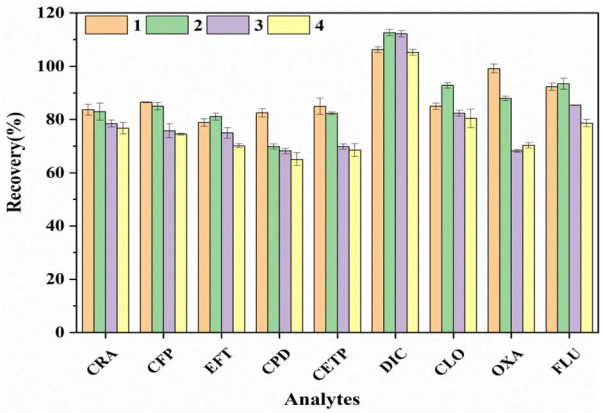

Fig. 5 Reusable times of Fe_3O_4@SiO_2@Ap-COF.

Table 1 Matrix effects of 9 β-LAs

	ME (%)	
Analytes	Water	Milk
CRA	85.3	98.2
CFP	94.5	110.7
EFT	100.5	114.7
CPD	94.7	109.0
CETP	99.9	105.8
DIC	118.2	114.9
CLO	113.8	112.4
OXA	115.5	114.8
FLU	115.8	110.7

Table 2 Analytical performance of the proposed MSPE-UPLC-MS/MS method for the determination of β-LAs

				LOD		LOQ	
Analytes	Linear range (μg L^{-1})	Calibration curve	R^2	Water (μg L^{-1})	Milk (μg kg^{-1})	Water (μg L^{-1})	Milk (μg kg^{-1})
CRA	0.2–200	$Y = 14\,007.8X + 2205.6$	0.9998	0.001	0.005	0.004	0.015
CFP	0.2–200	$Y = 3005.7X + 858.1$	0.9997	0.013	0.018	0.041	0.056
EFT	0.2–200	$Y = 25\,390.2X + 790.1$	0.9998	0.003	0.004	0.009	0.011
CPD	0.2–200	$Y = 918\,54X + 17\,470.8$	0.9997	0.001	0.002	0.002	0.006
CETP	0.2–200	$Y = 1\,432\,26X + 36\,026.3$	0.9995	0.001	0.003	0.003	0.008
DIC	0.2–200	$Y = 16\,412.7X + 7253.3$	0.9994	0.002	0.006	0.007	0.018
FLU	0.2–200	$Y = 28\,092.4X + 1298.7$	0.9996	0.007	0.006	0.020	0.019
CLO	0.2–200	$Y = 378.5X + 32.4$	0.9999	0.102	0.347	0.310	1.051
OXA	0.2–100	$Y = 27\,891.2X + 687.9$	0.9993	0.001	0.005	0.003	0.016

Therefore, hydrophobic interaction was also an important factor for the effective adsorption of β-LAs by Fe_3O_4@SiO_2@Ap-COF. In conclusion, the dominant adsorption mechanism of Fe_3O_4@SiO_2@Ap-COF with β-LAs involved π–π interaction, hydrogen bonding and hydrophobic interactions.

To further investigate the adsorption selectivity of Fe_3O_4@SiO_2@Ap-COF for β-LAs, the other two categories of antibiotics including nitroimidazoles (NMZs) and tetracyclines (TCs) were also tested. As seen in Table S4, Fe_3O_4@SiO_2@Ap-COF had low adsorption efficiency (<30%) for NMZs and TCs, exhibiting good adsorption selectivity towards β-LAs.

3.4 Reusability of the adsorbent

For MSPE adsorbents, it is very important to evaluate their reusability. Through reusing multiple times, the good adsorption performance is a key indicator of evaluating material's reusability.[18] In this experiment, Fe_3O_4@SiO_2@Ap-COF containing β-LAs was washed with 8 mL, 0.3% acidified methanol for several times, dried in vacuum at 60 °C for 4 h, and then several continuous adsorption–desorption tests were carried out to investigate the reusability of the adsorbent. As seen in Fig. 5, Fe_3O_4@SiO_2@Ap-COF could be reused for 4 times, and the recoveries of 9 β-LAs were all above 65%. The decline in adsorption efficiency after repeated use can be due to fouling from the analyzed sample. The results showed that Fe_3O_4@SiO_2@Ap-COF has good reusability.

3.5 Matrix effect

Matrix effect (ME) refers to influence of other co-extracted components in the sample matrix on the measurement of the target analyte, which can cause signal suppression or enhancement during UPLC-MS/MS analysis.[61] In this study, ME were assessed by the ratio of slopes between the matrix-matched calibration curves and the solvent calibration curves. ME could be ignored if the ratio was closer to 80–120%. The formula of ME is listed below:

$$\mathrm{ME}(\%) = \frac{\text{slope of calibration curve in matrix}}{\text{slope of calibration curve in solvent}} \times 100$$

The blank matrix solutions of surface water and milk blank matrix solutions without the target substances were obtained according to the sample pretreatment and MSPE steps, and the ME of 9 β-LAs were assessed at different concentrations. According to the calculation results (Table 1), the range of the ME of water and milk were respectively 85.3–118.2% and 98.2–114.9%, demonstrating that the tested analytes showed no obvious matrix effect. Therefore, to the sensitive and accurate determination of water and milk samples, we chose an external standard method using solvent standard curve for quantitative analysis in this experiment.

3.6 Method validation

3.6.1 Linearity, LODs, and LOQs. Under optimal conditions, the analytical performance of the developed method was investigated. The mixed standard solutions of 9 β-LAs were prepared at concentrations of 0.2, 0.5, 1, 2, 5, 10, 20, 50, 100, and 200 ng mL^{-1} using the initial mobile phase as the solvent. The corresponding standard curves were constructed by plotting the peak area of the analyte (*y*-axis) against the concentration (*x*-axis) for each analyte, yielding the corresponding linear equations and correlation coefficients (R^2). As seen in Table 2, in the range of 0.2–200 μg kg^{-1}, good linearity of 9 β-LAs was obtained with R^2 ranging from 0.9993 to 0.9999. The limit of detection (LOD) and limit of quantitation (LOQ) were defined as the lowest detectable concentration of analyte when signal-to-noise ratios were 3 and 10, respectively. LOD and LOQ were important indicators for assessing method sensitivity. As presented in Table 2, the LODs of 9 β-LAs in water and milk were 0.001–0.102 μg L^{-1} and 0.002–0.347 μg kg^{-1}, respectively; and the LOQs of 9 β-LAs in water and milk were 0.002–0.310 μg L^{-1} and 0.006–1.051 μg kg^{-1}, which proved that the method had high sensitivity.

3.6.2 Recovery and precision. To assess the accuracy and precision of the proposed method, spike recovery experiments were performed at three different standard concentrations levels: 0.4, 1.6, and 4 μg L^{-1}. As shown in Table S3, under three different spiked levels with 5 parallel experiments, good recoveries of 9 β-LAs were obtained in both water and milk samples, which were 78.2–118.1% and 71.7–118.8%, respectively; the relative standard deviation (RSD) values ranged from 1.14% to 9.46%, indicating high accuracy and precision of the method.

3.7 Method application in real samples

The method was applied to analyze 15 milk samples and 20 water samples. As a result, none of the target 9 β-LAs were detected.

4 Conclusions

In summary, a new core–shell magnetic material Fe_3O_4@-SiO_2@Ap-COF was synthesized, which exhibited good adsorption efficiency and selectivity for 9 β-LAs. Using this material as an MSPE adsorbent, a new method for determining 9 β-LAs in water and milk were developed. The method showed that the LODs were 0.001 μg L^{-1}–0.102 μg L^{-1} (water) and 0.002 μg kg^{-1}–0.347 μg kg^{-1} (milk), and the LOQs were 0.002 μg L^{-1}–0.310 μg L^{-1} (water) and 0.006 μg kg^{-1}–1.051 μg kg^{-1} (milk), respectively, with RSDs less than 9.46%, indicating high sensitivity, accuracy and precision, thus enabling the rapid, high-throughput determination of 9 β-LAs in water and milk.

Author contributions

Lu Li: writing – original draft, conceptualization, formal analysis, methodology. Na Li: data curation, formal analysis, methodology, writing – original draft. Wendan Niu: data curation, validation, investigation. Aijing Guo: methodology, validation. Ling Ma: conceptualization, supervision, funding acquisition. Wei Zhao: conceptualization, supervision. Yawei Zhang: conceptualization, supervision. Ke Wang: conceptualization, supervision, writing – review & editing, project administration, funding acquisition, resources. All authors have read and agreed to the published version of the manuscript.

Conflicts of interest

There are no conflicts to declare.

Data availability

The data supporting the findings of this study are available within the article and its supplementary information (SI). Supplementary information is available. See DOI: https://doi.org/10.1039/d5ra09307d.

Acknowledgements

This work was supported by the National Natural Science Foundation of China (81903322), S&T Program of Hebei (223777116D) and the funding for the Fourth Batch of Discipline Leading Talents in Shijiazhuang City.

References

1 Z. Huang, X.-D. Pan, B. Huang, J.-J. Xu, M.-L. Wang and Y.-P. Ren, *Food Control*, 2016, **66**, 145–150.
2 V. G. Alekseev, *Pharm. Chem. J.*, 2010, **44**, 14–24.
3 M. Cycoń, A. Mrozik and Z. Piotrowska-Seget, *Front. Microbiol.*, 2019, **10**, 338.
4 Y. M. Mesfin, B. A. Mitiku and H. Tamrat Admasu, *Vet. Med. Sci.*, 2024, **10**, e70049.
5 Y. Yang, Y. S. Ok, K.-H. Kim, E. E. Kwon and Y. F. Tsang, *Sci. Total Environ.*, 2017, **596–597**, 303–320.
6 V. Samanidou and S. Nisyriou, *J. Sep. Sci.*, 2008, **31**, 2068–2090.
7 T. A. H. Nguyen, T. N. M. Pham, T. B. Le, D. C. Le, T. T. P. Tran, T. Q. H. Nguyen, T. K. T. Nguyen, P. C. Hauser and T. D. Mai, *J. Chromatogr. A*, 2019, **1605**, 360356.
8 S. Ahmed, J. Ning, G. Cheng, M. K. Maan, T. Chen, I. Ahmad, S. A. Algharib and Z. Yuan, *Microchem. J.*, 2020, **152**, 104354.
9 M. Cámara, A. Gallego-Picó, R. M. Garcinuño, P. Fernández-Hernando, J. S. Durand-Alegría and P. J. Sánchez, *Food Chem.*, 2013, **141**, 829–834.
10 M. Iranifam and M. Khabbaz Kharameh, *Luminescence*, 2015, **30**, 625–630.
11 Q. Yang, Y. Liu, Z. Jiang, M. Xu, S. Yao, C. Li, G. Chen, M. Xu, W. Liu, L. Yin and Z. Hu, *Anal. Biochem.*, 2021, **631**, 114299.
12 J. Li, X. Ren, Y. Diao, Y. Chen, Q. Wang, W. Jin, P. Zhou, Q. Fan, Y. Zhang and H. Liu, *Food Chem.*, 2018, **257**, 259–264.
13 Y. Wang, X. Ma, Y. Peng, Y. Liu and H. Zhang, *J. Hazard. Mater.*, 2021, **416**, 126098.
14 R. B. Hoff, L. Molognoni, C. T. P. Deolindo, M. O. Vargas, C. R. Kleemann and H. Daguer, *J. Chromatogr. B*, 2020, **1152**, 122232.
15 S. Zhi, J. Zhou, H. Liu, H. Wu, Z. Zhang, Y. Ding and K. Zhang, *J. Chromatogr. B*, 2020, **1154**, 122286.
16 Y. Zhang, X. Xue, S. Su, Z. Guo, J. Wang, L. Ding, Y. Liu and J. Zhu, *Food Anal. Methods*, 2018, **11**, 2865–2884.
17 Q. Chen, X.-D. Pan, B.-F. Huang and J.-L. Han, *J. Pharm. Biomed. Anal.*, 2017, **145**, 525–530.
18 L. Li, Y. Yin, G. Zheng, S. Liu, C. Zhao, L. Ma, Q. Shan, X. Dai, L. Wei, J. Lin and W. Xie, *Arab. J. Chem.*, 2022, **15**, 103912.
19 S. A. Khatibi, S. Hamidi and M. R. Siahi-Shadbad, *Crit. Rev. Food Sci. Nutr.*, 2021, **61**, 3361–3382.
20 L. Xia, L. Liu, X. Lv, F. Qu, G. Li and J. You, *J. Chromatogr. A*, 2017, **1500**, 24–31.
21 L. Fu, H. Zhou, E. Miao, S. Lu, S. Jing, Y. Hu, L. Wei, J. Zhan and M. Wu, *Food Chem.*, 2019, **289**, 701–707.
22 X. He, G. N. Wang, K. Yang, H. Z. Liu, X. J. Wu and J. P. Wang, *Food Chem.*, 2017, **221**, 1226–1231.
23 M. Hernández-Mesa, C. Cruces-Blanco and A. M. García-Campaña, *Talanta*, 2017, **163**, 111–120.
24 H. Duo, X. Lu, X. Nie, L. Wang, S. Wang, X. Liang and Y. Guo, *J. Chromatogr. A*, 2020, **1626**, 461328.
25 T. Liu, C. Sang, Y. Liu, B. Shao and G. He, *Food Chem.*, 2025, **492**, 145624.
26 A. Azzouz, L. Hejji, A. Assafi and K.-H. Kim, *TrAC, Trends Anal. Chem.*, 2025, **193**, 118468.
27 N. Yuan, C. Zhang, X. Zhang and R. Zhang, *J. Cleaner Prod.*, 2024, **434**, 140259.
28 Z. Shen, X. Xu, X. Wang, Z. Du and F. Zhang, *Food Chem.*, 2025, **496**, 146712.
29 J. Ge, J. Xiao, L. Liu, L. Qiu and X. Jiang, *J. Porous Mater.*, 2016, **23**, 791–800.

30 K. Hu, Y. Shi, W. Zhu, J. Cai, W. Zhao, H. Zeng, Z. Zhang and S. Zhang, *Food Chem.*, 2021, **339**, 128079.
31 C. Zhang, G. Li and Z. Zhang, *J. Chromatogr. A*, 2015, **1419**, 1–9.
32 L. Wen, L. Liu, X. Wang, M.-L. Wang, J.-M. Lin and R.-S. Zhao, *J. Chromatogr. A*, 2020, **1625**, 461275.
33 N. Li, D. Wu, N. Hu, G. Fan, X. Li, J. Sun, X. Chen, Y. Suo, G. Li and Y. Wu, *J. Agric. Food Chem.*, 2018, **66**, 3572–3580.
34 P. N. Nomngongo, S. K. Selahle, A. Mpupa, A. Nqombolo, T. S. Munonde and L. M. Madikizela, *TrAC, Trends Anal. Chem.*, 2024, **179**, 117906.
35 J. Peng, D. Liu, T. Shi, H. Tian, X. Hui and H. He, *Anal. Bioanal. Chem.*, 2017, **409**, 4157–4166.
36 X. Yang, X. Zhou, Q. Wang, Q. Yang, J. Wang and L. Chen, *J. Chromatogr. A*, 2025, **1762**, 466341.
37 G. Wang, T. Zhou and Y. Lei, *RSC Adv.*, 2020, **10**, 11557–11564.
38 Q. Li, S. Zhu, F. Wu, F. Chen and C. Guo, *Microchim. Acta*, 2023, **190**, 369.
39 J. Xin, X. Wang, N. Li, L. Liu, Y. Lian, M. Wang and R.-S. Zhao, *Food Chem.*, 2020, **330**, 127255.
40 J. Li, M. Chen, Z. Gao, J. Du, W. Yang and M. Yin, *Colloids Surf. B Biointerfaces*, 2016, **146**, 468–474.
41 S. Lin, N. Gan, L. Qiao, J. Zhang, Y. Cao and Y. Chen, *Talanta*, 2015, **144**, 1139–1145.
42 M. A. Habila, Z. A. ALOthman, A. M. El-Toni, J. P. Labis and M. Soylak, *Talanta*, 2016, **154**, 539–547.
43 L. Lian, J. Lv, X. Wang and D. Lou, *J. Chromatogr. A*, 2018, **1534**, 1–9.
44 P. Shi and N. Ye, *Talanta*, 2015, **143**, 219–225.
45 Y. Hao, M. Yang, X. Chen, F. Zhang, N. Li, M. He and M. Xu, *J. Agric. Food Chem.*, 2023, **71**, 8656–8664.
46 X. Zhang, L. Chen, Y. Xu, H. Wang, Q. Zeng, Q. Zhao, N. Ren and L. Ding, *J. Chromatogr. B*, 2010, **878**, 3421–3426.
47 Y. Li, H. Zhang, Y. Chen, L. Huang, Z. Lin and Z. Cai, *ACS Appl. Mater. Interfaces*, 2019, **11**, 22492–22500.
48 N. Li, M. Liang, H. Zhang, Z. Hua, L. Ma, Y. Qi and K. Wang, *RSC Adv.*, 2024, **14**, 8303–8312.
49 D. Li, M. He, B. Chen and B. Hu, *J. Chromatogr. A*, 2019, **1601**, 1–8.
50 Y. Chen and Z. Chen, *Talanta*, 2017, **165**, 188–193.
51 D. Wei, A. Pan, C. Zhang, M. Guo, C. Lou, J. Zhang, H. Wu and X. Wang, *Food Chem.*, 2023, **404**, 134464.
52 M. Zhang, J. Li, C. Zhang, Z. Wu, Y. Yang, J. Li, F. Fu and Z. Lin, *J. Chromatogr. A*, 2020, **1615**, 460773.
53 M. Shirani, B. Akbari-adergani, H. Rashidi Nodeh and S. Shahabuddin, *Microchim. Acta*, 2020, **187**, 634.
54 R. Mirzaei, M. Yunesian, S. Nasseri, M. Gholami, E. Jalilzadeh, S. Shoeibi, H. S. Bidshahi and A. Mesdaghinia, *J. Environ. Health Sci. Eng.*, 2017, **15**, 21.
55 H. Su, Y. Lin, Z. Wang, Y.-L. E. Wong, X. Chen and T.-W. D. Chan, *J. Chromatogr. A*, 2016, **1466**, 21–28.
56 D. Li, J. Zhu, M. Wang, W. Bi, X. Huang and D. D. Y. Chen, *J. Chromatogr. A*, 2017, **1491**, 27–35.
57 F. J. Lara, M. Del Olmo-Iruela, C. Cruces-Blanco, C. Quesada-Molina and A. M. García-Campaña, *TrAC, Trends Anal. Chem.*, 2012, **38**, 52–66.
58 R. Li, Y. Zhu, X. Zhang, S. Li, D. Wang, Z. Liu, X. Wang, Y. Hou and S. Li, *Polymer*, 2025, **320**, 127973.
59 N. Wang, H. Li, D. Kong, X. Feng, C. Li, X. Cui and T. Wang, *Dyes Pigm.*, 2025, **240**, 112841.
60 M. S. Islam and S. Mitra, *Hybrid Adv.*, 2023, **3**, 100074.
61 J. Wu, E. Guo, M. Wang, K. Wang, L. Ma and K. Lian, *J. Food Compos. Anal.*, 2023, **122**, 105437.